Improved transfer efficiencies in radio-frequency-driven recoupling solid-state NMR by adiabatic sweep through the dipolar recoupling condition

Author(s):
Straasø, Lasse A.; Shankar, Ravi; Tan, Kong O.; Hellwagner, Johannes; Meier, Beat H.; Hansen, Michael R.; Nielsen, Niels C.; Vosegaard, Thomas; Ernst, Matthias; Nielsen, Anders B.

Publication date:
2016

Permanent link:
https://doi.org/10.3929/ethz-b-000119017

Originally published in:
The Journal of Chemical Physics 145(3), https://doi.org/10.1063/1.4958318

Improved Transfer Efficiencies in Radio-Frequency-Driven Recoupling Solid-State NMR by Adiabatic Sweep through the Dipolar Recoupling Condition

Lasse A. Straasø,[1] Ravi Shankar,[1] Kong Ooi Tan,[2] Johannes Hellwagner,[2] Beat H. Meier,[2] Michael Ryan Hansen,[3] Niels Chr. Nielsen,[1] Thomas Vosegaard,[1] Matthias Ernst[2] and Anders B. Nielsen[1,*]

[1]Interdisciplinary Nanoscience Center (iNANO) and Department of Chemistry, Aarhus University, Gustav Wieds Vej 14, DK-8000 Aarhus C, Denmark.

[2] Physical Chemistry, ETH Zürich, Vladimir-Prelog-Weg 2, 8093 Zürich, Switzerland.

[3]Institute of Physical Chemistry, Westfälische Wilhelms-Universität Münster, Corrensstrasse 28/30, D-48149 Münster, Germany.

*Corresponding author: Anders B. Nielsen (abn@inano.au.dk)

The homonuclear radio-frequency driven recoupling (RFDR) experiment is commonly used in solid-state NMR spectroscopy to gain insight into the structure of biological samples due to its ease of implementation, stability towards fluctuations/missetting of radio-frequency (rf) field strength, and in general low rf requirements. A theoretical operator-based Floquet description is presented to appreciate the effect of having a temporal displacement of the π-pulses in the RFDR experiment. From this description, we demonstrate improved transfer efficiency for the RFDR experiment by generating an adiabatic passage through the zero-quantum (ZQ) recoupling condition. We have compared the performances of RFDR and the improved sequence to mediate efficient ^{13}CO to $^{13}C_{\alpha}$ polarization transfer for uniformly ^{13}C,^{15}N-labeled glycine and for the fibril forming peptide SNNFGAILSS uniformly ^{13}C,^{15}N-labeled at the FGAIL residues. Using numerically optimized sweeps, we get experimental gains of approximately 20 % for glycine where numerical simulations predict an improvement of 25% relative to the standard implementation. For the fibril forming peptide, using the same sweep parameters as found for glycine, we have gains in the order of 10 to 20 % depending on the spectral regions of interest.

KEYWORDS: Solid-state NMR spectroscopy, homonuclear dipolar recoupling, RFDR, Floquet Theory, polarization transfer, adiabatic passage.

This manuscript was accepted by J. Chem. Phys. Click here to see the version of record.

Introduction

Homonuclear dipolar recoupling techniques are essential building blocks in biological solid-state magic-angle-spinning (MAS) NMR spectroscopy.[1-3] These techniques provide access to important structural information which is otherwise averaged by MAS[4] that is required to obtain high-resolution spectra. In multidimensional experiments, the dipolar recoupling blocks are routinely used to identify nuclei which are close in proximity, thereby facilitating resonance assignment or gathering of distance restraints[5]. This approach has been used as a key component in structure determination of numerous biological macromolecules.[6,7]

A large variety of homonuclear dipolar recoupling techniques have been developed over the years[1-3]. Many of these sequences rely on the reintroduction of a so-called effective double-quantum (DQ) Hamiltonian, like the homonuclear rotary resonance (HORROR)[8] sequence, different symmetry-based experiments[9] and the back-to-back (BaBa) experiment[10] to mention a few. Each of these experiments has different properties, making the particular experimental conditions the decisive factor for which sequence to use. An important criterion for the recoupling element is the overall transfer efficiency, which generally can be improved by generating an adiabatic passage through the recoupling condition[11]. An example where such a passage has increased the efficiency is the dipolar recoupling enhancement through amplitude modulation (DREAM) experiment[12]. In DREAM, the radio-frequency (rf) field amplitude is swept through the HORROR[8] matching condition, thereby allowing a theoretical transfer efficiency of 100% compared to 73% for the HORROR experiment in powder samples.

Another class of homonuclear recoupling sequences reintroduces a zero-quantum (ZQ) Hamiltonian. While the DQ Hamiltonian gives negative peaks for the direct transfer and consecutively positive and negative peaks for relayed transfers, the ZQ Hamiltonian always gives positive correlation peaks and, hence, avoids the risk of cancellation of signal in case of overlapping resonance frequencies for relayed transfers. Radio-frequency driven recoupling (RFDR)[13-15] is a commonly used technique for generating a ZQ Hamiltonian since it is easy to implement and has relatively low demands on the rf-field amplitude.

In resonance assignment experiments of biological samples, several transfer steps often occur and it is important to optimize each individual step. In particular, the ^{13}CO to $^{13}C_{\alpha}$ transfer has been a limiting step when the MAS frequency is lower than the chemical-shift difference between the two carbon resonances of interest. Under these experimental conditions, the rotational resonance tickling scheme[16] (R_2T) cannot be employed as the CSA tensor will also be recoupled. Thus, the polarization transfer is often done by employing second-order schemes like proton-driven spin diffusion (PDSD)[17] and variants hereof or by dipolar recoupling techniques like RFDR or the band-selective homonuclear CP (BSH-CP)[18] experiment.

In this paper, we present a modification of the RFDR sequence with improved transfer efficiency mediated by an adiabatic passage through the resonance condition, hereby, ideally achieving transfer efficiencies up to 100%. This is conceptually different from the previous modification to improve the stability of the RFDR experiment which replaces the hard π-pulses by adiabatic inversion pulses.[19] Such a modification will only change the efficiency of the inversion pulses but not the efficiency of the RFDR experiment. We have embedded the RFDR sequence in a 2D experiment as illustrated in Fig. 1a. The original sequence employs one π-pulse in the center of every rotor period as seen from Fig. 1b. A XY-4 or XY-8 phase-cycling scheme[20,21] of the pulse train leads to improved stability of the experiment towards chemical-shift offsets and pulse imperfections since certain higher-order terms of the Hamiltonian are averaged[21]. Additionally, we have implemented ^1H decoupling with constant x-phase for all ^1H pulses but with rf field strength of $\omega_{pul}/2\pi$ during the ^{13}C π-pulses and $\omega_{win}/2\pi$ during the windows between them which has been shown to improve the transfer performance. [15]

Figure 1

By varying the temporal placement of the π-pulses, we can selectively reintroduce the chemical-shifts with a variable scaling factor during the homonuclear dipolar recoupling period. A schematic representation of the sequence is given in Fig. 1c. Here, we are using two rotor periods as basic unit with the two π-pulses time-shifted by $\Delta\tau$ in opposite directions relative to the times $\frac{\tau_r}{2}$ and $\frac{3\tau_r}{2}$,

respectively. In the following, we define $\Delta\tau$ to be negative when the first pulse is shifted to start before $\frac{\tau_r}{2}$ and being positive if the first pulse is shifted to start after $\frac{\tau_r}{2}$ and vise versa for the second pulse. A specific time-shift is repeated four times to use the XY-8 phase-cycling scheme (x,y,x,y,y,x,y,x) for the π-pulses.[21] To mimic an adiabatic passage through the recoupling condition, the time-shift $\Delta\tau$ is changed gradually. Note that for $\Delta\tau = 0\,\mu s$, we reproduce the RFDR experiment.

We first address the theoretical background, then we demonstrate improved performance through numerical simulations and finally we present supporting experimental results obtained by focusing on the ^{13}CO to $^{13}C_\alpha$ polarization transfer on U-^{13}C,^{15}N-labeled glycine and for the fibril forming peptide SNNFGAILSS uniformly ^{13}C,^{15}N-labeled at the FGAIL residues[22] (henceforth referred to as FGAIL).

Theory

For a theoretical description of the experiment, let us consider two homonuclear coupled spin-1/2 nuclei, I_1 and I_2. In the usual rotating (Zeeman) frame, the time-dependent Hamiltonian including isotropic and anisotropic chemical-shift interactions and the dipole-dipole coupling of the system under MAS and rf irradiation is given by

$$\hat{H}(t) = +\hat{H}_I(t) + \hat{H}_{II}(t) + \hat{H}_{\mathrm{rf}}(t) \tag{1}$$

with

$$\hat{H}_I(t) = \sum_{q=1}^{2}\sum_{n=-2}^{2} \omega_{\mathrm{I}_q}^{(n)} e^{in\omega_r t}\hat{I}_{qz}\,, \tag{2}$$

$$\hat{H}_{II}(t) = \sum_{n=-2}^{2} \omega_{\mathrm{I}_1\mathrm{I}_2}^{(n)} e^{in\omega_r t}\left(2\hat{I}_{1z}\hat{I}_{2z} - \hat{I}_{1x}\hat{I}_{2x} - \hat{I}_{1y}\hat{I}_{2y}\right)\,, \tag{3}$$

where the angular frequencies $\omega_{I_1}^{(n)}$ and $\omega_{I_2}^{(n)}$ are the isotropic ($n=0$) and anisotropic ($n\neq 0$) chemical-shifts, $\omega_{I_1I_2}^{(n)}$ the dipolar coupling, ω_r the spinning frequency, q denotes either spin 1 or 2, and $\hat{I}_{qj}$ (j=x,y,z) denotes the different spin operator components for spin q. For simplicity, we will restrict the description to the case of ideal π-pulses. In the rf toggling frame, the dipolar coupling Hamiltonian in Eq. (3) is unchanged but the chemical-shift Hamiltonian in Eq. (2) can be written as

$$\hat{\tilde{H}}_I(t)=\sum_{q=1}^{2}\sum_{n=-2}^{2}\omega_{I_q}^{(n)}e^{in\omega_r t}\Phi(t)\hat{I}_{qz}, \tag{4}$$

where $\Phi(t)$ denotes the sign of the chemical-shift Hamiltonian at a given time. It depends on the number of applied π-pulses, M, as $\Phi(t)=(-1)^M$.

As discussed in previous papers on the RFDR experiment[13,14], it is the isotropic chemical-shift difference which recouples the dipolar coupling Hamiltonian. Thus, we rewrite the effective isotropic chemical-shift as $\omega_{I_1}^{(0)}\Phi(t)\hat{I}_{1z}+\omega_{I_2}^{(0)}\Phi(t)\hat{I}_{2z}=\Delta\Omega\Phi(t)\hat{I}_z^{ZQ}+\sum\Omega\Phi(t)\hat{I}_z^{DQ}$ with $\left(\omega_{I_1}^{(0)}-\omega_{I_2}^{(0)}\right)=\Delta\Omega$ and $\left(\omega_{I_1}^{(0)}+\omega_{I_2}^{(0)}\right)=\sum\Omega$ denoting the difference or the sum of the isotropic chemical-shift, respectively. We have also introduced the fictitious ZQ and DQ operators for the terms in relation to the isotropic chemical-shift interaction with $\hat{I}_z^{ZQ}=\frac{1}{2}\left(\hat{I}_{1z}-\hat{I}_{2z}\right)$ and $\hat{I}_z^{DQ}=\frac{1}{2}\left(\hat{I}_{1z}+\hat{I}_{2z}\right)$[23].

The adiabatic RFDR experiment is implemented by a time-shift of the π-pulses such that the position of the first π-pulse (in the first rotor period) is at $\tau_r/2+\Delta\tau$ and the second (in the second rotor period) at $\tau_r/2-\Delta\tau$. The time-modulation of $\Delta\Omega\Phi(t)$ due to the π–pulses is shown in Fig. 2a. Before transforming the description into the ZQ chemical-shift interaction frame, it proves worthwhile to separate $\Delta\Omega\Phi(t)$ into an average, time-independent part and a time-dependent part with zero net phase over a full cycle. The same description has recently been proposed to analyze amplitude-modulated rf

fields[24]. The time-independent part of the chemical-shift difference is given by $\Delta\Omega_{CW} = \overline{\Delta\Omega\,\Phi(t)}$, where the bar denotes the time average. Schematically, the average, time-independent shift is shown on the right in Fig. 2b. The time-dependent component with zero net phase angle is then given by $\Delta\Omega_m(t) = \Delta\Omega\,\Phi(t) - \Delta\Omega_{CW}$ and is shown to the left in Fig. 2b. Using these definitions, Eq. (4) takes the form

$$\hat{\tilde{H}}_I(t) = \Delta\Omega_m(t)\hat{I}_z^{ZQ} + \Delta\Omega_{CW}\hat{I}_z^{ZQ} + \sum\Omega\,\Phi(t)\hat{I}_z^{DQ} + \sum_{q=1}^{2}\sum_{n=-2,n\neq 0}^{2}\omega_{I_q}^{(n)}e^{in\omega_r t}\Phi(t)\hat{I}_{qz}\,. \tag{5}$$

In Eq. (5), the chemical-shift Hamiltonian is split into several terms which commute and can be treated separately in an interaction-frame transformation. An interaction-frame transformation by the time-dependent component of the isotropic chemical-shift difference Hamiltonian, $\Delta\Omega_m(t)\hat{I}_z^{ZQ}$, can be described by the transformation operator

$$\hat{U}(t) = e^{-i\int_0^t \Delta\Omega_m(t')\hat{I}_z^{ZQ}dt'} = e^{-i\beta(t)\hat{I}_z^{ZQ}} \tag{6}$$

with $\cos(\beta(t)) = \sum_{k=-\infty}^{\infty} a_k^x e^{ik\omega_m t}$ and $\sin(\beta(t)) = \sum_{k=-\infty}^{\infty} a_k^y e^{ik\omega_m t}$, where $\beta(t)$ defines the phase angle calculated by direct integration of $\Delta\Omega_m(t)$, and a_k^x and a_k^y are the Fourier coefficients of the interaction-frame transformation and k is an integer. The interaction-frame dipolar coupling Hamiltonian can then be written as a Fourier series with two characteristic frequencies as

$$\begin{aligned}\hat{\tilde{H}}_{II}(t) &= \hat{U}^{\dagger}(t)\hat{H}_{II}(t)\hat{U}(t)\\ &= e^{i\beta(t)\hat{I}_z^{ZQ}}\sum_{n=-2}^{2}\omega_{I_1I_2}^{(n)}e^{in\omega_r t}\left(2\hat{I}_{1z}\hat{I}_{2z} - \hat{I}_{1x}\hat{I}_{2x} - \hat{I}_{1y}\hat{I}_{2y}\right)e^{-i\beta(t)\hat{I}_z^{ZQ}}\\ &= \sum_{n=-2}^{2}\sum_{k=-\infty}^{\infty}\hat{\tilde{H}}_{II}^{(n,k)}e^{in\omega_r t}e^{ik\omega_m t}.\end{aligned} \tag{7}$$

The Fourier components $\hat{\tilde{H}}_{II}^{(n,k)}$ are given by

$$\begin{aligned}\hat{\tilde{H}}_{II} &= -\left(\hat{I}_{1x}\hat{I}_{2x}+\hat{I}_{1y}\hat{I}_{2y}\right)\omega^{(n)}_{\mathrm{I_1I_2}}a^{x}_{k}+\left(\hat{I}_{1y}\hat{I}_{2x}-\hat{I}_{1x}\hat{I}_{2y}\right)\omega^{(n)}_{\mathrm{I_1I_2}}a^{y}_{k}+\left\{\omega^{(n)}_{\mathrm{I_1I_2}}2\hat{I}_{1z}\hat{I}_{2z}\right\}\delta_{k,0}\\ &= -\hat{I}^{\mathrm{ZQ}}_{x}\omega^{(n)}_{\mathrm{I_1I_2}}a^{x}_{k}+\hat{I}^{\mathrm{ZQ}}_{y}\omega^{(n)}_{\mathrm{I_1I_2}}a^{y}_{k}+\left\{\omega^{(n)}_{\mathrm{I_1I_2}}2\hat{I}_{1z}\hat{I}_{2z}\right\}\delta_{k,0},\end{aligned} \tag{8}$$

where we express the dipolar coupling interaction using the fictitious ZQ operators[23] with $\hat{I}^{\mathrm{ZQ}}_{x}=\hat{I}_{1x}\hat{I}_{2x}+\hat{I}_{1y}\hat{I}_{2y}$ and $\hat{I}^{\mathrm{ZQ}}_{y}=\hat{I}_{1y}\hat{I}_{2x}-\hat{I}_{1x}\hat{I}_{2y}$. For n = 0, we have $\hat{\tilde{H}}^{(0,k)}_{II}=0$ due to the setting of the magic angle.

The resonance conditions, based on the interaction-frame Hamiltonian from Eq. (7), is generally given by[25]

$$n\omega_{\mathrm{r}}+k\omega_{\mathrm{m}}=0, \tag{9}$$

where the values of n are restricted to ±1 and ±2, while k can take any integer value. For the basic element consisting of two π–pulses (two rotor periods), the modulation frequency is given by $\omega_{\mathrm{m}}=\frac{1}{2}\omega_{r}$ and we obtain from an operator-based Floquet[25] description the first-order effective dipolar coupling Hamiltonian in the time-modulated differential ZQ chemical-shift frame as

$$\hat{\tilde{H}}^{(1)}_{II}=\hat{\tilde{H}}^{(\pm1,\mp2)}_{II}+\hat{\tilde{H}}^{(\pm2,\mp4)}_{II}=-\hat{I}^{\mathrm{ZQ}}_{x}\sum_{2n+k=0}\omega^{(n)}_{\mathrm{I_1I_2}}a^{x}_{k}+\hat{I}^{\mathrm{ZQ}}_{y}\sum_{2n+k=0}\omega^{(n)}_{\mathrm{I_1I_2}}a^{y}_{k}=-\hat{I}^{\mathrm{ZQ}}_{x}\omega^{\mathrm{eff}}_{x}+\hat{I}^{\mathrm{ZQ}}_{y}\omega^{\mathrm{eff}}_{y}\ , \tag{10}$$

where the sum is taken over all possible values of n and k that contribute to the resonance condition given in Eq. (9). The variables $\omega^{\mathrm{eff}}_{x}$ and $\omega^{\mathrm{eff}}_{y}$ are short-hand notations of $\sum_{2n+k=0}\omega^{(n)}_{\mathrm{I_1I_2}}a^{x}_{k}$ and $\sum_{2n+k=0}\omega^{(n)}_{\mathrm{I_1I_2}}a^{y}_{k}$, respectively. To determine the effective dipole-dipole coupling strength, we define

$$\omega_{eff}\left(\alpha_{PR},\beta_{PR},\gamma_{PR}\right)=\sqrt{\left(\sum_{2n-k=0}\omega^{(n)}_{\mathrm{I_1I_2}}a^{x}_{k}\right)^{2}+\left(\sum_{2n-k=0}\omega^{(n)}_{\mathrm{I_1I_2}}a^{y}_{k}\right)^{2}}\ . \tag{11}$$

Figure 2c displays the calculated magnitude of the first-order effective dipolar coupling Hamiltonian as a function of the time shift $\Delta\tau$ relative to the effective dipole-dipole coupling strength

of the standard RFDR experiment, $\omega_{\text{eff}}^{\text{RFDR}}$, which is recovered for $\Delta\tau = 0$ μs. Powder averaging has been performed as

$$\omega_{\text{eff}} = \frac{1}{8\pi^2}\int \omega_{\text{eff}}\left(\alpha_{\text{PR}},\beta_{\text{PR}},\gamma_{\text{PR}}\right)\sin(\beta_{\text{PR}})d\alpha_{\text{PR}}d\beta_{\text{PR}}d\gamma_{\text{PR}}, \tag{12}$$

where the three Euler angles α_{PR}, β_{PR}, and γ_{PR} denote angles defining the transformation between the principal axis system and the rotor-fixed frame. The calculation has been accomplished by setting $|\Delta\Omega|/2\pi = 1.2\omega_{\text{r}}/2\pi = 12$ kHz which corresponds to about 120 ppm chemical-shift difference for two ^{13}C nuclei on a 400 MHz spectrometer at 10.0 kHz MAS. From Fig. 2c, it can be seen that the effective dipolar coupling strength is zero when $\frac{\Delta\tau}{\tau_r} = \pm 0.5$. These conditions correspond to having both π-pulses on top of each other or separated by two rotor periods and no recoupling will happen. By setting $\frac{\Delta\tau}{\tau_r} = 0$, the normal RFDR sequence is recovered. It is clear that for small time-shifts, the effective dipolar coupling strength is not changing significantly and that the mean scaling factor is symmetric around the standard RFDR condition ($\Delta\tau = 0$ μs). It should also be mentioned that aiming for the highest transfer efficiency does not necessarily match the condition for the strongest effective dipolar coupling as, for instance, the interplay between the residual differential chemical-shift interaction and the recoupled dipolar coupling interaction complicates the picture. Furthermore, the profile is highly dependent on the relative ratio of the chemical-shift difference and the spinning frequency and, hence, new calculations have to be done when changing the before-mentioned parameters.

Figure 2

At this point, we can write up the effective first-order Hamiltonian containing both the time-independent isotropic and anisotropic chemical-shift, and the dipolar coupling Hamiltonian

$$\hat{\bar{H}}^{(1)} = \Delta\Omega_{CW}\hat{I}_z^{\text{ZQ}} + \sum\Omega\Phi(t)\hat{I}_z^{\text{DQ}} - \omega_x^{\text{eff}}\hat{I}_x^{\text{ZQ}} + \omega_y^{\text{eff}}\hat{I}_y^{\text{ZQ}} + \hat{\bar{H}}_{\text{CSA}}^{(1)}, \tag{13}$$

with $\hat{H}^{(1)}_{\mathrm{CSA}} = \sum_{q=1}^{2}\sum_{n=-2,n\neq 0}^{2} \omega^{(n)}_{\mathrm{I}q}\, 4(-1)^{(n+1)} \frac{\sin\left(n\omega_{\mathrm{r}}\Delta\tau\right)}{n\omega_{\mathrm{r}}} I_{qz}$. Neglecting the chemical-shift anisotropy, it is evident from Eq. (13) that by changing the time-shift $\Delta\tau$ and thereby changing $\Delta\Omega_{\mathrm{CW}} = \left(\omega^{(0)}_{\mathrm{I}_1} - \omega^{(0)}_{\mathrm{I}_2}\right)\frac{2\Delta\tau}{\tau_r}$ proportionally, the effective axis of rotation in a ZQ subspace will change with $\Delta\Omega_{\mathrm{CW}}$ being the size of the z-axis component and the powder dependent effective dipolar coupling being the size of the x,y-plane component. In principle, this change can be sufficiently slowly to drag the polarization via an adiabatic passage through the recoupling condition such the density operator can be changed from $\hat{I}_{1z}$ to $\hat{I}_{2z}$. In reality, a compromise for the required mixing time is needed in order to get the highest transfer efficiency as relaxation effects also occur.

The size (or scaling factor) of the recoupled dipolar Hamiltonian in Eq. (10) is highly dependent on the ratio between the chemical-shift difference and the spinning frequency via the a_k^x and a_k^y Fourier coefficients which take the maximum value for k being around the value $\frac{|\Delta\Omega_{\mathrm{m}}(t)|}{\omega_{\mathrm{m}}}$ for the normal RFDR sequence as discussed for xix decoupling.[25] Hence, by having found good sweep parameters at a particular MAS frequency and chemical-shift offset setting, e.g. for 10 kHz MAS and 12 kHz chemical-shift difference for ^{13}CO to ^{13}C$_\alpha$ transfer on a 400 MHz spectrometer, one may use these parameters to find an approximately proper setting at 20 kHz MAS and a chemical-shift difference of 24 kHz on a 800 MHz spectrometer where the recoupled dipolar Hamiltonian will have the same scaling and then the individual time-shift $\Delta\tau$ should be half to keep the ZQ subspace and the dragging in a similar fashion.

As the anisotropic chemical-shifts also contribute to the sweep according to Eq. (13), the optimal sweeps are difficult to predict and a numerical approach can be pursued to optimize these. In the Supplementary Material,[26] a script that can be executed via SIMPSON to find the best sweeps via a grid search has been provided. Here, the finite pulse effect of the π-pulses is incorporated by making them last a time τ_π and calculation of the temporal placement is realized by allowing a sweep in a tangential

form of $\Delta\tau$ throughout the sequence with two parameters deciding the sweep size and form and one parameter governing the number of XY-8 elements in total. The displacement can be calculated according to

$$x = \left(-1 + 2\frac{i-1}{N-1} \right) tco, \quad i = 1,..,N \tag{14}$$

$$\Delta\tau = \frac{\tau_{\text{sweep}}}{2} \frac{\tan(x)}{\tan(tco)}, \tag{15}$$

with the sweep size denoted τ_{sweep}, the tangential cut-off angle denoted *tco* and N refers to the number of block repetitions. Here, we have used same notation for the parameters as given by Chandran et al.[27] If $N = 1$, then $\Delta\tau = 0$ μs is chosen as in standard RFDR.

To find the first delay, $\tau^{1,\text{prior}}$, up to the π pulse in the first rotor period in the *i*'th block, we calculate initially $\Delta\tau$. Equipped with $\Delta\tau$, the π-pulse should start at

$$\tau^{1,\text{prior}} = \tau_{\text{r}} / 2 + \Delta\tau - \tau_{\pi} / 2 \ . \tag{16}$$

To account for a finite π-pulse, half its duration is subtracted. Initially ($i = 1$), $\Delta\tau$ is negative in Eq. (16) when having positive values for τ_{sweep} and *tco* as seen in Eqs. (14) and (15). However, in general it should not matter if the sweep is in one direction or the other. The delay up to the second rotor period is then given by $\tau^{1,\text{after}} = \tau_{\text{r}} - \tau^{1,\text{prior}} - \tau_{\pi}$. The second delay, $\tau^{2,\text{prior}}$, up to the π-pulse in the second rotor period can be calculated as

$$\tau^{2,\text{prior}} = \tau_{\text{r}} / 2 - \Delta\tau - \tau_{\pi} / 2, \tag{17}$$

again taking the finite π-pulse duration into account. The residual delay in the second rotor period is $\tau^{2,\text{after}} = \tau_{\text{r}} - \tau^{2,\text{prior}} - \tau_{\pi}$. Since the general idea dictates to temporally shift the relative placement of only two π-pulses, we can extend the above delays according to the phase cycling, e.g., the XY-8 scheme. To get a feeling of the calculations, we have listed the calculated delays for the initial two rotor periods for

$\tau_\pi = 5\,\mu\text{s}$, $\tau_{\text{sweep}} = 2.5\,\mu\text{s}$, $\tau_{tp} = 100\,\text{ns}$, and $N = 2$. Thus, we obtain

$$\tau^{1,\text{prior}} - \tau_\pi - \tau^{1,\text{after}} - \tau^{2,\text{prior}} - \tau_\pi - \tau^{2,\text{after}} = 46.25\,\mu\text{s} - 5\,\mu\text{s} - 48.75\,\mu\text{s} - 48.75\,\mu\text{s} - 5\,\mu\text{s} - 46.25\,\mu\text{s}. \quad (18)$$

It should be mentioned that for N equal to 1, 2, and 3, the tangential cut-off angle has no effect, i.e., the form of the sweep is immaterial. For $N = 1$, then $\Delta\tau = 0$ µs; for $N = 2$, then $\Delta\tau = -\tau_{\text{sweep}}/2$ and $\Delta\tau = \tau_{\text{sweep}}/2$; for $N = 3$, then $\Delta\tau = -\tau_{\text{sweep}}/2$, $\Delta\tau = 0$ µs and $\Delta\tau = \tau_{\text{sweep}}/2$.

Numerical Simulations

All simulations were done using the open-source SIMPSON[28,29] software. Powder averaging was accomplished using the REPULSION[30] scheme with 66 α_{CR}, β_{CR} crystallite angles and 9 γ_{CR} angles. The ^{1}H Larmor frequency was set to 400 MHz and the MAS frequency to 10 kHz. The simulations were based on a representative ^{13}CO-^{13}C$_\alpha$ spin-pair in a polypeptide with the ^{13}C chemical-shift parameters $(\delta_{\text{iso}}^{\text{CS}}, \delta_{\text{aniso}}^{\text{CS}}, \eta^{\text{CS}}, \alpha_{\text{PE}}^{\text{CS}}, \beta_{\text{PE}}^{\text{CS}}, \gamma_{\text{PE}}^{\text{CS}})$ set as ^{13}CO (170 ppm, -76 ppm, 0.9, 0°, 0°, 90°) and ^{13}C$_\alpha$ (50 ppm, -20 ppm, 0.43, 90°, 90°, 0°) and the dipole-dipole coupling parameters $(b_{I_1I_2}/2\pi, \beta_{\text{PE}}, \gamma_{\text{PE}})$ set as (-2142 Hz, 90°, 120.8°)[31]. The subscript PE signifies the transformation from the principal axis frame to the peptide plane. The carrier was set in the middle of the spectrum (at 110 ppm). The starting operator and detection operator were set to longitudinal spin order ($\hat{I}_{1z} \rightarrow \hat{I}_{2z}$), π-pulses lasting 5 µs were implemented in the XY-8 phase scheme, and perfect ^{1}H heteronuclear decoupling was assumed in all simulations. Time-shifting was realized as described in the Theory section.

Grid search optimizations were performed to get the most suitable τ_{sweep} and *tco* parameters for a fixed number N of XY-8 block repetitions. The resulting parameters are displayed in Table 1. Specific adiabatic RFDR time-settings are provided upon request. To get an idea of the robustness of the sequence against the isotropic chemical-shifts, grid calculations were performed for a mixing time of 24 rotor periods (N = 3) and 80 rotor periods (N = 10) by varying the shift of ^{13}CO by ±10 ppm and the

shift of $^{13}C_\alpha$ by ±20 ppm.

N	1	2	3	4	5	6	7	8	9	10
τ_{sweep}/μs	0	2.9	2.5	3.2	3.3	3.4	3.7	3.5	3.7	3.6
tco/degrees	NaN	NaN	NaN	89	80	80	79	79	81	81

Table 1: The optimal adiabatic parameters (τ_{sweep}, *tco*) obtained in a grid search as function of the number of XY-8 element blocks (N). Note that the sweep form, i.e. *tco*, is immaterial for N = 1, 2, and 3.

Experimental

Parameters common to all experiments are addressed initially followed by sample-specific parameters for uniformly ^{13}C,^{15}N-labeled glycine and subsequently for the fibril forming peptide SNNFGAILSS uniformly ^{13}C,^{15}N-labeled at the FGAIL residues (FGAIL).

All experiments were conducted on a Bruker 400 Avance II NMR spectrometer (Bruker BioSpin, Rheinstetten, Germany) using a standard triple-resonance 2.5 mm MAS probe. The magic-angle setting was done on KBr[32] and the MAS frequency was set to 10 kHz. Referencing of resonances was done relative to tetramethylsilane (TMS) using adamantane as a secondary reference with $^{13}C_{low\text{-}field}$ at 38.48 ppm[33] and ^1H at 1.85 ppm[34]. In general, data were obtained with the ^1H carrier at 1.75 ppm and the ^{13}C carrier at 110 ppm using 3 s repetition delays in the pulse sequence presented in Fig. 1a. π-pulses of 5 μs duration were used in the XY-8 phase scheme to mediate polarization transfer. The XY-8 phase cycling was reset prior to each scan. The specific delays prior and after the π-pulses were implemented using the in-built variable pulse-list feature of the Bruker pulse programmer and used to define the width of the window ^1H decoupling periods with rf field strength of $\omega_{win}/2\pi$. To enhance sensitivity, cross-polarization (CP)[35] was used with a ramp[36] from 70-100% on the ^1H channel. All ^{13}C π/2-pulses had a duration of 2.5 μs. During acquisition, unified two pulse decoupling UTPD(φ,τ_1,,τ_2)[37] was applied. The actual setting can be read in the parameter set in parenthesis with the first parameter

denoting the phase shift between the two pulses, the second and third parameter denoting the length of the first and second pulse, respectively. TPPI was used to make the 2D experiments phase sensitive. Processing was done in Topspin 3.2 (Bruker Biospin, Rheinstetten, Germany) and zeroth- and first-order phase corrections were imposed manually after Fourier transformation.

The experimental data presented in Fig. 4 were extracted from 2D data for uniformly ^{13}C,^{15}N-labeled glycine obtained at ambient temperature. The ^{1}H excitation pulse duration was set to 3.0 µs and CP was used with a contact time of 0.5 ms and average rf field amplitudes of 85 kHz (^{1}H) and of 75 kHz (^{13}C). The adiabatic sweep timing (τ_{sweep}) was 2.5 µs, cf. Eqs. (14)-(17). In Fig. 4a and 4b the RFDR mixing time was increased in steps of four rotor periods from 0 to 24 while ^{1}H decoupling during the mixing elements was applied fulfilling $\omega_{pul}/2\pi$ = 150 kHz and $\omega_{win}/2\pi$ = 90 kHz. In Fig. 4c the rf field strength of the ^{1}H decoupling pulses during the π-pulses on ^{13}C channel was varied while keeping the windowed ^{1}H decoupling elements with constant rf field strength of $\omega_{win}/2\pi$ = 90 kHz. The mixing time was 1.2 ms for the normal RFDR experiment and 2.4 ms (N=3) for the adiabatic RFDR sequence. In Fig. 4d, the rf field strength of the ^{1}H decoupling during the window between the π-pulses on ^{13}C channel was varied while keeping constant rf field strength for the decoupling during the π-pulses of $\omega_{pul}/2\pi$ = 150 kHz. The mixing time was 1.2 ms for the normal RFDR experiment and 2.4 ms (N=3) for the adiabatic RFDR sequence. During acquisition, UTPD(170°,0.97τ_r,1.03τ_r) decoupling with rf amplitude of 87 kHz was applied. Each 2D spectrum employed 180 increments and a spectral width of 240 ppm ($t_{1,max}$ equal to 3.7 ms) in the indirect dimension. 8 transients (and 8 dummy scans) were used to fulfill the complete phase cycling in 8 steps. During processing, the 2D data sets were zero-filled to 4096 and 512 in the direct and indirect dimension, respectively, and no line broadening was applied. Routines in Topspin 3.2 were applied to extract a slice at 176.7 ppm in the indirect dimension. Likewise, Topspin 3.2 procedures were used to calculate integrals in the extracted slice after having performed automatic baseline correction. The integral regions covered 20 ppm, each centered at the

resonance frequencies of ^{13}CO (176.7 ppm) and $^{13}C_\alpha$ (43.5 ppm), respectively. Comparison of integrals across more spectra was rendered possible by normalizing all integrals against a specific value.

The experimental data presented in Fig. 5 were extracted from 2D data for FGAIL obtained at a temperature of approximately 278 K. The ^1H excitation pulse was set to 3.25 µs and CP was used with a contact time of 1.0 ms and average rf fields of 85 kHz (^1H) and of 75 kHz (^{13}C). In total, four experiments were recorded. For the normal RFDR and the adiabatic version, the mixing time was 12 and 24 rotor periods, respectively, which were experimentally found to give the highest transfer efficiencies and data from these are presented in Fig. 5. The adiabatic version used a τ_{sweep} of 2.5 µs. ^1H decoupling during the mixing elements was applied fulfilling $\omega_{pul}/2\pi$ = 150 kHz and $\omega_{win}/2\pi$ = 90 kHz. In the Supplementary Material[26] two additional slices are presented from spectra which were recorded under same conditions but by employing the normal RFDR experiment with a mixing time of 2.4 ms and one without any mixing element. During acquisition, UTPD(170°,0.97τ_r,1.03τ_r) decoupling with rf field strength of 87 kHz was applied. Each 2D spectrum employed 248 increments and a spectral width of 440 ppm ($t_{1,max}$ = 11.6 ms) in the indirect dimension. 32 transients were used to fulfill the complete phase cycling in 16 steps. Compared to the glycine experiments, an additional phase cycle of the last ^{13}C π/2 pulse was invoked. During processing, linear prediction using LPfc was applied with NCOEF=100 and the 2D data sets were zero-filled to 4096 and 1024 in the direct and indirect dimension, respectively, and the signals were apodized with a squared cosine function (SSB = 2.5). Routines in Topspin were applied to sum slices between 165.9 ppm to 178.0 ppm in the indirect dimension. Likewise, Topspin procedures were used to calculate integrals in the resulting 1D spectra after having performed automatic baseline correction. Comparison of integrals across more spectra was rendered possible by normalizing all integrals against the diagonal region from the spectrum without any mixing element.

Results and Discussion

Aiming at finding the most efficient ^{13}CO to $^{13}C_\alpha$ transfer at a 400 MHz spectrometer using 10.0 kHz MAS, the optimal sweep parameters were numerically found as described in the Numerical Simulation section and the optimal parameters for different mixing times can be found in Table 1. In Fig. 3a, the numerical calculated transfer efficiencies for RFDR (blue squares) and the different optimal adiabatic RFDR (red squares) sequences are compared. The ^{13}CO to $^{13}C_\alpha$-transfer efficiency is indeed increasing as expected when an adiabatic passage through the resonance condition is getting closer to be realized and the curve clearly shows that an adiabatic passage can nearly be accomplished with approximately 79% transfer efficiency at mixing time of 8 ms. At a 400 MHz spectrometer, normal RFDR turns out in simulations to reach a maximum transfer of 53.3% after 24 rotor periods (N = 3). For the same mixing time, the adiabatic version of RFDR transfers more than 66.7%, corresponding to an improvement of 25% relative to the standard implementation.

Figure 3

During the adiabatic sweep, the effective axis of rotation in ZQ subspace is given by a combination of the induced isotropic and anisotropic chemical-shift differences. Changing the isotropic chemical-shifts relative to each other will, therefore, provide some insight into the robustness towards the chemical-shifts values often encountered in biological samples. The resulting contour plots are given for RFDR in Fig. 3b employing a mixing time of 24 rotor periods (N = 3), adiabatic RFDR in Fig. 3c employing a mixing time of 24 rotor periods (N = 3) and adiabatic RFDR in Fig. 3d employing a mixing time of 80 rotor periods (N = 10). From the plots based on the adiabatic RFDR sequences, it is evident that the polarization transfer is higher over the entire chemical shift region compared to the ordinary RFDR sequence. In addition, the variation of the transfer efficiency is very small in the plotted chemical-shift regions. Combined, these observations illustrate that even though the effective z-axis of rotations is changed in the ZQ subspace due to changes in the differential isotropic chemical-shifts, the

adiabatic passage is still working very efficiently and the adiabatic version is in general better than the standard.

Figure 4 presents a comparison of the experimental transfer efficiencies for ordinary RFDR (blue squares and crosses) and the adiabatic RFDR sequence (red squares and crosses) which was optimized for $N = 3$. The transfer efficiencies have been extracted as indicated in the Experimental section from slices of 2D spectra recorded on U-^{13}C,^{15}N -labeled glycine at 10.0 kHz MAS on a 400 MHz spectrometer. In Figs. 4a and 4b are the peak intensities of cross peaks and diagonal peaks as function of mixing time presented. The mixing time has been increased in steps of four rotor periods in order to find the maximal transfer efficiency for the normal RFDR sequence which may not require the full phase-cycling as the buildup time for the highest transient depends on the scaling factor of the recoupled dipolar Hamiltonian. The peak intensities have been integrated and normalized to the diagonal peak intensity from a spectrum without any mixing element. The adiabatic RFDR is recorded consistently with τ_{sweep} equal to 2.5 µs. Hence, only the last measured data point (after 24 rotor periods with $N = 3$) exploits the entire sweep of the given sequence which is different from what is presented in Fig. 3a where individually transfer efficiencies for full sweeps are simulated for different mixing times. From the data in Fig. 4a, it is seen that the transfer efficiency is increasing as more elements are employed for the adiabatic RFDR sequence and finally an approximately 55% transfer efficiency is reached which corresponds to a gain of more than 20 % over ordinary RFDR which reaches a transfer efficiency of approximately 45% after 12 rotor periods. The inset in right lower corner in Fig. 4a shows spectrum slices extracted from the highest ^{13}CO to $^{13}C_{\alpha}$ cross peaks for RFDR (blue) and adiabatic RFDR (red). It can be seen that the signal-to-noise ratio is really good, and, from the reference spectrum (without any mixing time) the signal-to-noise ratio has been determined to be more than 6000. It can be seen in Fig. 4b that the diagonal peak intensity is continuously dropping throughout the entire adiabatic sweep whereas for the normal sequence, it is more like that the polarization is equilibrating between the two carbon atoms. This equilibration after more than 12 rotor periods of mixing time is due to the different effective dipolar coupling strengths for a powder sample where polarization will be transferred

either forward or backward for certain crystallites. The less dominant diagonal peak intensity at maximum transfer for the adiabatic RFDR sequence (at 24 rotor periods) compared to the ordinary RFDR sequence (at 12 rotor periods) may be useful in case the element is used to mediate polarization transfer among aliphatic carbon atoms where a strong diagonal peak may interfere and complicate peak assignment.

Figure 4

From the experimental data presented in Figs. 4a and 4b, an adiabatic passage through the resonance condition is not fulfilled as the mixing time is too short for this. However, for $N = 3$ we still receive a compensation of the angle-dependency as seen from the numerical simulations in Fig. 3a. By increasing the length of the adiabatic version we did not find any additional gain in the experimentally transfer efficiencies which in general is lower than presented in the numerical simulations (55% compared to 66.7%) in Fig. 3a. This may be explained by several aspects that we have not discussed in the Theory section. First of all, the numerical simulations were performed for an isolated two-spin system without relaxation which does not describe the full spin dynamics in a multi-spin system. In particular, insufficient ^{1}H decoupling under the mixing element will decrease the performance. It has been discussed that better decoupling performance may be achieved using moderate CW irradiation during the windows between the π-pulses and strong CW during the π-pulses.[15] In Fig. 4c we present experimental data for the peak intensities of cross peaks as function of the ^{1}H rf field strength $\omega_{pul}/2\pi$ during the π-pulses on the ^{13}C pulses. In general, the performance is increasing with stronger decoupling field during the π-pulses and the increase is higher for the adiabatic version of RFDR compared to the normal version. This finding may be caused by the fact that the overall mixing time is increased from 12 to 24 rotor periods for the RFDR to the adiabatic RFDR sequence. In Fig. 4d, the cross peaks intensities as function of ^{1}H decoupling strength during the windows between the π-pulses are presented. The data are recorded using a total mixing time of 12 rotor periods for RFDR and 24 rotor periods for the adiabatic version with $\omega_{pul}/2\pi$ = 150 kHz. From the data, it is seen that the transfer efficiency is indeed

not sensitive towards the ^{1}H decoupling in the windowed periods for both RFDR experiments. Hence, in order to achieve best performance it is worth to use different decoupling rf field strengths during the mixing element to reduce the overall rf consumption. A full theoretical description of decoupling performance is beyond the scope of this article.

Another reason for getting less transfer experimentally compared to that achieved in the simulations may be that by changing the position of the π-pulses, we partly reintroduce not only the anisotropic chemical-shift but also heteronuclear dipolar coupling interactions. By applying sufficiently efficient ^{1}H decoupling this will not pose a problem to the protons but the ^{13}C-^{15}N dipole-dipole couplings will still be active. However, no experimental gain was found by applying low-power CW rf irradiation on the ^{15}N channel during the mixing element. Currently, we are also investigating whether pulse imperfections, i.e., phase transients and finite amplitude rising times influence the transfer efficiency. Compensation of such experimental imperfections might make it possible to realize additional gain in the efficiency of the (adiabatic) RFDR sequence.

The transfer performance of the adiabatic RFDR sequence has also been compared to the ordinary RFDR sequence on basis of 2D ^{13}C-^{13}C correlation spectra of SNNFGAILSS amyloid fibrils uniformly ^{13}C,^{15}N-labeled at the FGAIL residues. The pulse sequences were optimized for highest $^{13}C_{\alpha}$ cross peak intensities. The data are presented in Fig. 5. The 2D spectrum shown in Fig. 5a has been obtained utilizing the adiabatic RFDR sequence with a mixing time of 24 rotor periods (N = 3). All experimental parameters can be found in the Experimental section. From the spectrum it is seen that polarization transfer is achieved not only for ^{13}CO to $^{13}C_{\alpha}$ and reverse but also among aliphatic side-chain carbons, clearly illustrating the broadband features of the adiabatic RFDR sequence covering the entire ^{13}C spectral region.

Figure 5

Elaborating on the ^{13}CO,$^{13}C_{\alpha}$-transfer, the integrated rows in the carbonyl region from 165.9 ppm to 178.0 ppm in the indirect dimension of the 2D spectra using either RFDR (with a mixing time of

1.2 ms) or the adiabatic RFDR render it possible to directly compare the two methods. The resulting 1D spectra are given in Figs. 5b and 5c, respectively, and the numbers highlighted in each spectrum relate to integrated signal intensities for the regions marked by the arrows relative to the diagonal carbonyl peak from a 2D spectrum without any mixing element. We note that we also recorded the normal RFDR experiment using a mixing time of 2.4 ms. The result can be found in the Supplementary Material[26] but was found to be worse than using 1.2 ms of mixing time. Consistently, the new adiabatic RFDR technique shows gains in the order of 10-20% depending on the chemical-shift region of interest. Note that the peaks at around 20 ppm arising from transfer of carbonyl polarization to side-chains nuclei have not been included in the analysis, however, for these side-chains the adiabatic sequence is improving the intensity relative to the ordinary RFDR sequence, mainly due to a longer mixing time. This clearly illustrates why we choose a short adiabatic RFDR sequence with a mixing time of 24 rotor periods (N = 3) as to minimize relayed polarization transfer. By including the entire aliphatic region in the analysis, the total transfer efficiency was found to be approximately 53% for the adiabatic RFDR sequence compared to 43% for the RFDR sequence which corresponds to a gain of around 20%.

Conclusions

In conclusion, we have presented an adiabatic variant of the RFDR experiment significantly improving polarization transfer by gradually changing the temporal positions of the π-pulses throughout the mixing time. Theoretically, the modifications can be understood by realizing that the non-averaged chemical-shift difference can be swept such that an adiabatic passage through the zero-quantum recoupling condition can be accomplished, thereby dragging the polarization from one nucleus to another. Experimentally, we have shown that the technique is indeed improving the transfer efficiency for ^{13}CO to $^{13}C_{\alpha}$ polarization transfer compared to the conventional RFDR sequence. At present, the optimal sweep parameters are found numerically as the sweep through the resonance condition is affected by the isotropic as well as the anisotropic chemical-shift differences of the involved nuclei and, therefore, depend on the particular characteristics of the spin system. However, the presented sweeps

can be used to guide optimizations for other experimental settings for $^{13}CO_2$ to $^{13}C_\alpha$ polarization transfer by scaling the time-shift $\Delta\tau$ accordingly to keep the relative sizes of the x,y and z components in the ZQ subspace the same.

Supplementary Material

See Supplementary Material at [URL][26] for a SIMPSON script that via a grid search provides optimized adiabatic sweep parameters.

Acknowledgment

We would like to thank Johannes Wittmann for stimulating discussions. Support from the Danish Council for Independent Research (DFF-4090-00223), the Villum Foundation under the Young Investigator Program (VKR023122), the Swiss National Science Foundation (Grants 200020_124611 and 200020_134681) and the ETH Zürich (Grant ETH-10 15-1), the Danish National Research Foundation (DNRF 0059), Carlsbergfondet, Aarhus University, and the Danish Ministry of Higher Education and Science (AU-2010-612-181) is gratefully acknowledged.

References

1 Griffin, R. G. Dipolar recoupling in MAS spectra of biological solids. *Nature structural biology* **5**, 508-512 (1998).

2 Ladizhansky, V. Homonuclear dipolar recoupling techniques for structure determination in uniformly 13C-labeled proteins. *Solid State Nuclear Magnetic Resonance* **36**, 119-128 (2009).

3 Nielsen, N. C., Strassø, L. A. & Nielsen, A. B. Dipolar Recoupling. *Topics in Current Chemistry* **306**, 1-47 (2012).

4 Andrew, E. R., Bradbury, A. & Eades, R. G. Removal of Dipolar Broadening of Nuclear Magnetic Resonance Spectra of Solids by Specimen Rotation. *Nature* **183**, 1802-1803 (1959).

5 Schuetz, A., Wasmer, C., Habenstein, B., Verel, R., Greenwald, J., Riek, R., Böckmann, A. & Meier, B.H. Protocols for the Sequential Solid-State NMR Spectroscopic Assignment of a Uniformly Labeled 25 kDa Protein: HET-s(1-227). *ChemBioChem* **11**, 1543-1551 (2010).

6 McDermott, A. Structure and Dynamics of Membrane Proteins by Magic Angle Spinning Solid-State NMR. *Annual Review of Biophysics* **38**, 385-403 (2009).

7 Comellas, G. & Rienstra, C. M. Protein Structure Determination by Magic-Angle Spinning Solid-State NMR, and Insights into the Formation, Structure, and Stability of Amyloid Fibrils. *Annual Review of Biophysics* **42**, 515-536 (2013).

8 Nielsen, N. C., Bildsoe, H., Jakobsen, H. J. & Levitt, M. H. Double-Quantum Homonuclear Rotary Resonance - Efficient Dipolar Recovery in Magic-Angle-Spinning Nuclear-Magnetic-Resonance. *Journal of Chemical Physics* **101**, 1805-1812 (1994).

9 Levitt, M. H. Symmetry in the design of NMR multiple-pulse sequences. *Journal of Chemical Physics* **128**, 052205-052230 (2008).

10 Feike, M., Demco, D. E., Graf, R., Gottwald, J., Hafner, S. & Spiess, H. W. Broadband Multiple-Quantum NMR Spectroscopy. *Journal of Magnetic Resonance, Series A* **122**, 214-221 (1996).

11 Ernst, M. & Meier, B. H. in *eMagRes* (John Wiley & Sons, Ltd, 2007).

12 Verel, R., Ernst, M. & Meier, B. H. Adiabatic dipolar recoupling in solid-state NMR: The DREAM scheme. *Journal of Magnetic Resonance* **150**, 81-99 (2001).

13 Bennett, A. E., Ok, J. H., Griffin, R. G. & Vega, S. Chemical-Shift Correlation Spectroscopy in Rotating Solids - Radio Frequency-Driven Dipolar Recoupling and Longitudinal Exchange. *Journal of Chemical Physics* **96**, 8624-8627 (1992).

14 Bennett, A. E., Rienstra, C. M., Griffith, J. M., Zhen, W. G., Lansbury, P. T. & Griffin, R. G. Homonuclear radio frequency-driven recoupling in rotating solids. *Journal of Chemical Physics* **108**, 9463-9479 (1998).

15 Bayro, M. J., Ramachandran, R., Caporini, M. A., Eddy, M. T. & Griffin, R. G. Radio frequency-driven recoupling at high magic-angle spinning frequencies: Homonuclear recoupling sans heteronuclear decoupling. *Journal of Chemical Physics* **128**, 052321 (2008).

16 Costa, P. R., Sun, B. Q. & Griffin, R. G. Rotational resonance tickling: Accurate internuclear distance measurement in solids. *Journal of the American Chemical Society* **119**, 10821-10830 (1997).

17 Szeverenyi, N. M., Sullivan, M. J. & Maciel, G. E. Observation of Spin Exchange by Two-Dimensional Fourier-Transform C-13 Cross Polarization-Magic-Angle Spinning. *Journal of Magnetic Resonance* **47**, 462-475 (1982).

18 Chevelkov, V., Shi, C., Fasshuber, H. K., Becker, S. & Lange, A. Efficient band-selective homonuclear CO–CA cross-polarization in protonated proteins. *Journal of Biomolecular NMR* **56**, 303-311 (2013).

19 Leppert, J., Heise, B., Ohlenschläger, O., Görlach, M. & Ramachandran, R. Broadband RFDR with adiabatic inversion pulses. *Journal of Biomolecular NMR* **26**, 13-24 (2003).

20 Maudsley, A. A. Modified Carr-Purcell-Meiboom-Gill sequence for NMR fourier imaging applications. *Journal of Magnetic Resonance (1969)* **69**, 488-491 (1986).

21 Gullion, T. & Schaefer, J. Elimination of resonance offset effects in rotational-echo, double-resonance NMR. *Journal of Magnetic Resonance (1969)* **92**, 439-442, (1991).

22 Nielsen, J. T., Bjerring, M., Jeppesen, M. D., Pedersen, R. O., Pedersen, J. M., Hein, K. L., Vosegaard, T., Skydstrup, T., Otzen, D. E. & Nielsen, N. C. Unique Identification of Supramolecular Structures in Amyloid Fibrils by Solid-State NMR Spectroscopy. *Angewandte Chemie-International Edition* **48**, 2118-2121 (2009).

23 Vega, S. Fictitious spin-1/2 operator formalism for multiple quantum NMR. *Journal of Chemical Physics* **68**, 5518-5527 (1978).

24 Nielsen, A. B., Tan, K. O., Shankar, R., Penzel, S., Cadalbert, R., Samoson, A., Meier, B. H. & Ernst, M. Theoretical description of RESPIRATION-CP. *Chemical Physics Letters* **645**, 150-156 (2016).

25 Scholz, I., van Beek, J. D. & Ernst, M. Operator-based Floquet theory in solid-state NMR. *Solid State Nuclear Magnetic Resonance* **37**, 39-59 (2010).

26 Supplementary Material

27 Vinod Chandran, C., Madhu, P. K., Kurur, N. D. & Bräuniger, T. Swept-frequency two-pulse phase modulation (SWf-TPPM) sequences with linear sweep profile for heteronuclear decoupling in solid-state NMR. *Magnetic Resonance in Chemistry* **46**, 943-947 (2008).

28 Bak, M., Rasmussen, J. T. & Nielsen, N. C. SIMPSON: A general simulation program for solid-state NMR spectroscopy. *Journal of Magnetic Resonance* **147**, 296-330 (2000).

29 Tošner, Z., Andersen, R., Stevensson, B., Edén, M., Nielsen, N. C. & Vosegaard, T. Computer-intensive simulation of solid-state NMR experiments using SIMPSON. *Journal of Magnetic Resonance* **246**, 79-93 (2014).

30 Bak, M. & Nielsen, N. C. REPULSION, A Novel Approach to Efficient Powder Averaging in Solid-State NMR. *Journal of Magnetic Resonance* **125**, 132-139 (1997).

31 Bak, M., Schultz, R., Vosegaard, T. & Nielsen, N. C. Specification and visualization of anisotropic interaction tensors in polypeptides and numerical simulations in biological solid-state NMR. *Journal of Magnetic Resonance* **154**, 28-45 (2002).

32 Frye, J. S. & Maciel, G. E. Setting the magic angle using a quadrupolar nuclide. *Journal of Magnetic Resonance (1969)* **48**, 125-131 (1982).

33 Morcombe, C. R. & Zilm, K. W. Chemical shift referencing in MAS solid state NMR. *Journal of Magnetic Resonance* **162**, 479-486 (2003).

34 Hayashi, S. & Hayamizu, K. Chemical Shift Standards in High-Resolution Solid-State NMR (1) ^{13}C, ^{29}Si, and ^{1}H Nuclei. *Bulletin of the Chemical Society of Japan* **64**, 685-687 (1991).

35 Schaefer, J. & Stejskal, E. O. Carbon-13 Nuclear Magnetic Resonance of Polymers Spinning at the Magic Angle. *Journal of the American Chemical Society* **98**, 1031-1032 (1976).

36 Metz, G., Wu, X. L. & Smith, S. O. Ramped-Amplitude Cross-Polarization in Magic-Angle-Spinning Nmr. *Journal of Magnetic Resonance Ser A* **110**, 219-227 (1994).

37 Equbal, A., Bjerring, M., Madhu, P. K. & Nielsen, N. C. A unified heteronuclear decoupling strategy for magic-angle-spinning solid-state NMR spectroscopy. *Journal of Chemical Physics* **142**, 184201 (2015).

Figure 1

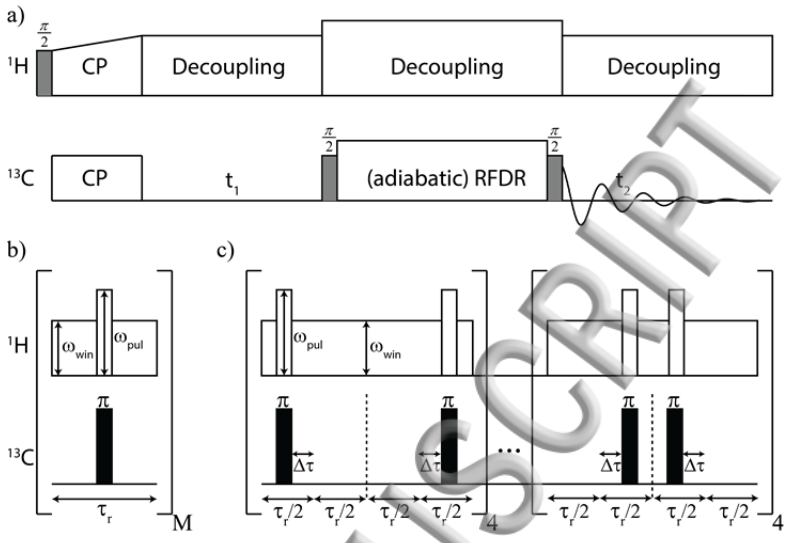

Fig. 1. (a) Schematic representation of a 2D ^{13}C-^{13}C correlation experiment using either (b) RFDR or (c) adiabatic RFDR to mediate polarization transfer. The RFDR element consists of one π-pulse centered in the middle of each rotor period. This element is then repeated M times. In adiabatic RFDR, two rotor periods are considered where the temporal positions of the pulses are moved in opposite directions with respect to the center by time Δτ. A given time-change is repeated four times to employ a XY-8 phase cycling of the π-pulses. The element is then repeated with a new value for the time Δτ. Black bars represent π-pulses while the gray bars represent $\frac{\pi}{2}$-pulses. During the RFDR mixing element, ^{1}H decoupling with constant x-phase is employed with rf field strength of $\omega_{pul}/2\pi$ during the π-pulses and $\omega_{win}/2\pi$ during the windows between them.

Figure 2

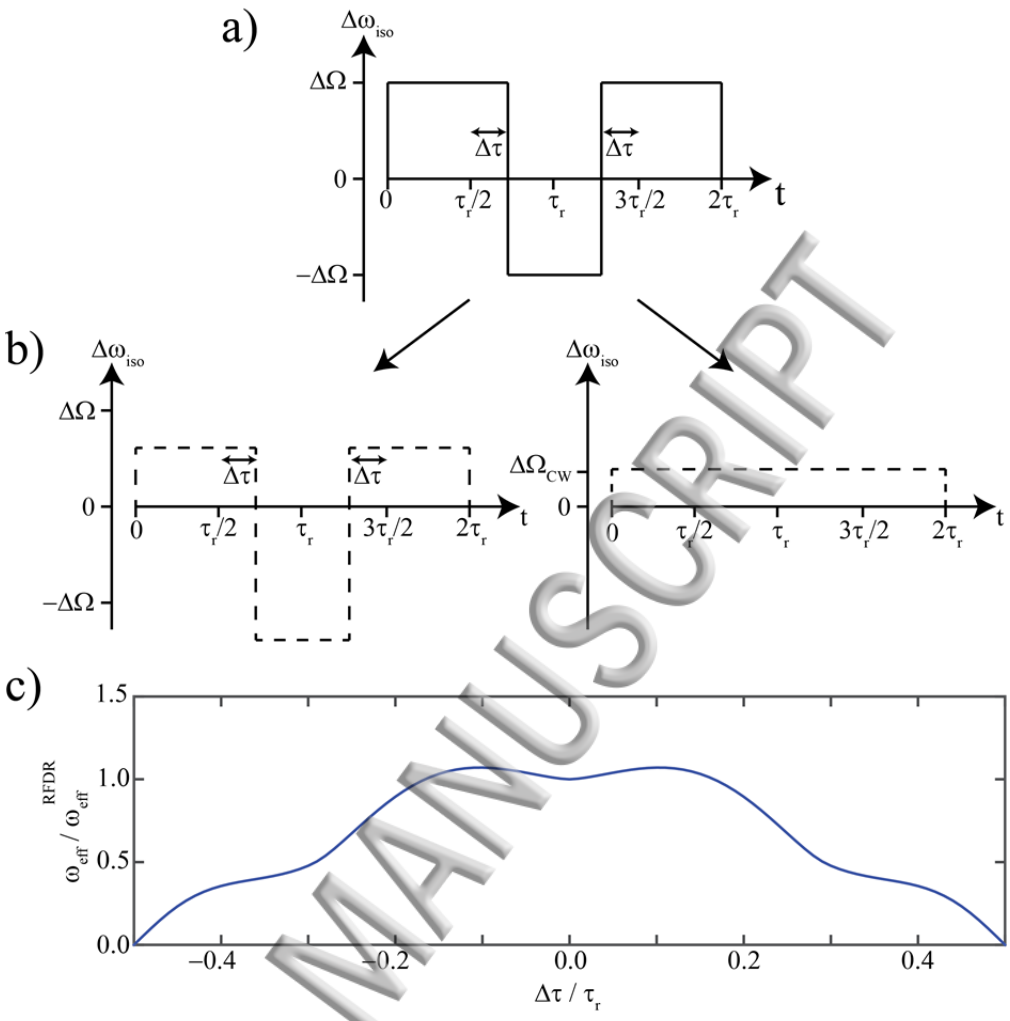

Fig. 2. (a) The time-evolution of the isotropic chemical-shift difference $\left(\omega_{I_1}^{(0)} - \omega_{I_2}^{(0)}\right)\Phi(t) = \Delta\Omega\Phi(t)$ between the two nuclei of interest can be separated into (b, left) a time-dependent component $\Delta\Omega_m(t) = \Delta\Omega\Phi(t) - \Delta\Omega_{CW}$ and (b, right) an average, time-independent part $\Delta\Omega_{CW} = \overline{\Delta\Omega\Phi(t)}$ where we have chosen a positive $\Delta\tau$ for the first π-pulse. This corresponds to the last part of the sweep in Fig. 1c. In (c), a plot of the powder averaged strength for the recoupled dipolar Hamiltonian (Eqs. (11) and (12)) is given as function of the relative time-shift Δτ of the π-pulses. The strength is scaled to unity for $\Delta\tau = 0$. The calculation is done by setting $|\Delta\Omega|/2\pi = 1.2\omega_r/2\pi = 12$ kHz.

Figure 3

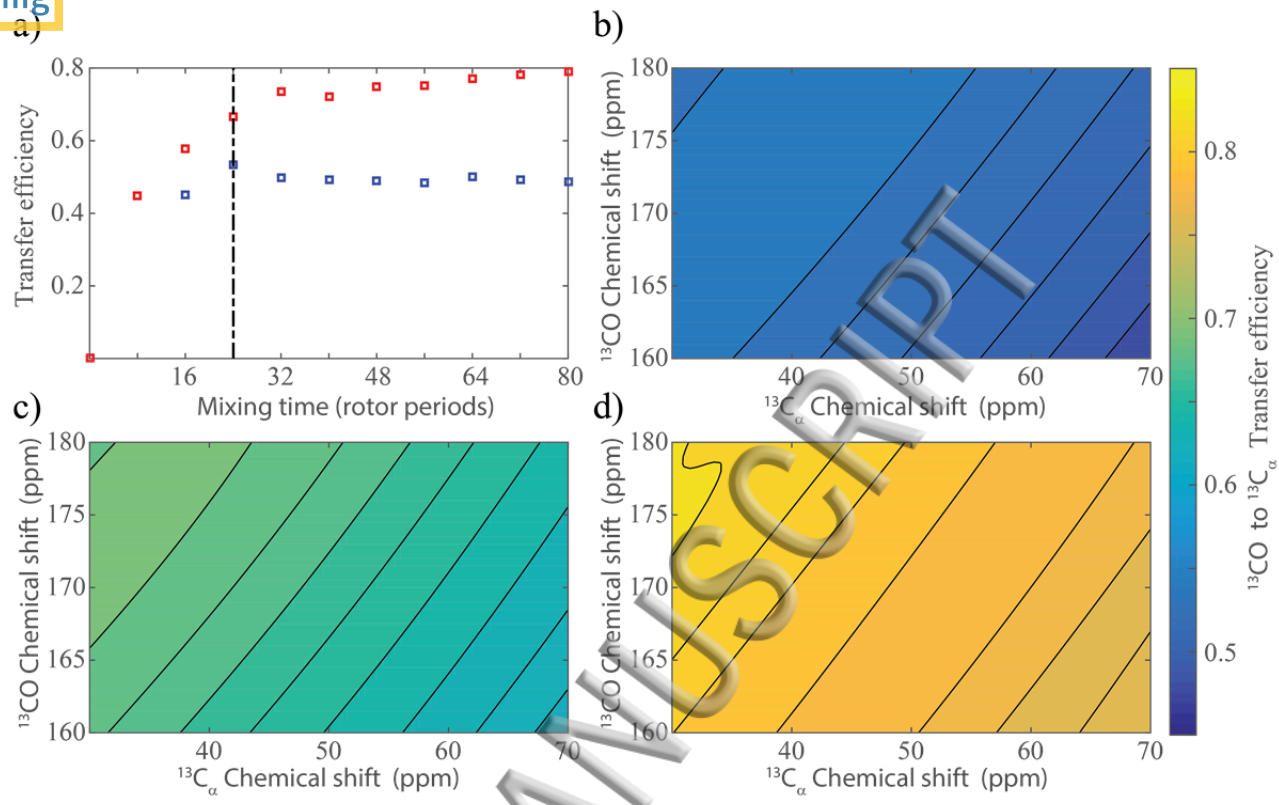

Fig. 3. (a) Simulations for the transfer efficiencies for RFDR (blue squares) and adiabatic RFDR (red squares) as function of mixing time. For a given number of blocks, *N*, the corresponding time-shifts and tangential sweep forms of the most efficient adiabatic RFDR sequence has been selected. Dashed line at *N*=3 indicates the time-point of maximum transfer efficiency of standard RFDR. The transfer efficiency as function of chemical-shifts for both involved nuclei are numerical calculated for (b) RFDR (with *N*=3), (c) adiabatic RFDR (with *N*=3) and (d) adiabatic RFDR (with *N*=10). All simulations were done for a 400 MHz spectrometer at 10.0 kHz MAS. The rf field strength of the π-pulses was set to 100 kHz and a XY-8 phase cycling was employed. Additional parameters for all simulations and time-sweep for the adiabatic RFDR sequence are given in the Numerical Simulation section.

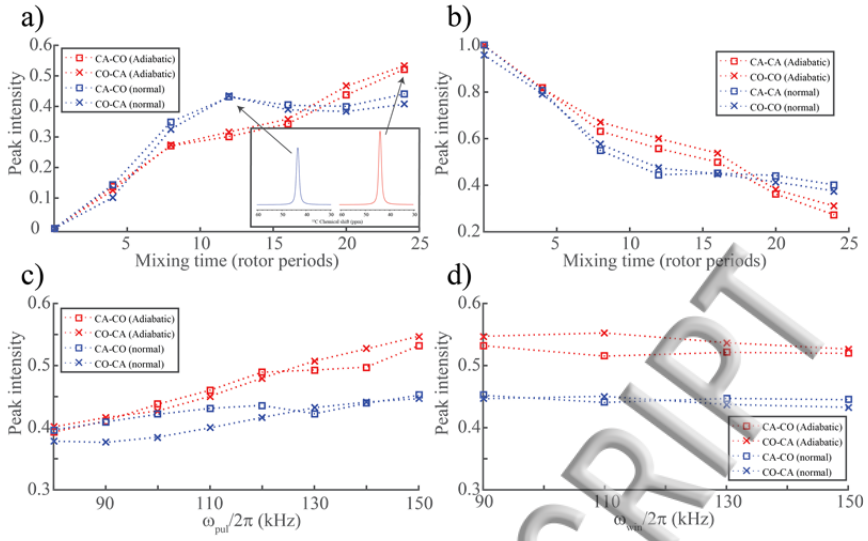

Fig. 4. Extracted experimental peak intensities (relative to initial diagonal peaks without any mixing element) from 2D spectra on U-^{13}C,^{15}N -labeled glycine using RFDR (blue crosses and squares) and adiabatic RFDR (red crosses and squares). In (a) signal intensities of cross peaks and (b) diagonal peaks as function of mixing time are presented. ^{1}H decoupling was employed during the mixing elements using $\omega_{pul}/2\pi$ = 150 kHz and $\omega_{win}/2\pi$ = 90 kHz. Note, for the adiabatic RFDR points, the entire sweep is only executed at a mixing time of 24 rotor periods (N=3). The inset in right lower corner of (a) shows spectrum slices for highest ^{13}CO to ^{13}C$_\alpha$ cross peaks for RFDR (blue) and adiabatic RFDR (red). In (c) cross peaks intensities as function of ^{1}H decoupling strength during the π-pulses with $\omega_{win}/2\pi$ = 90 kHz and (d) cross peaks intensities as function of ^{1}H decoupling strength during the windows between the π-pulses with $\omega_{pul}/2\pi$ = 150 kHz is presented using a total mixing time of 12 rotor periods for RFDR and 24 rotor periods for the adiabatic version. All peak intensities have been scaled relative to the diagonal peak from a 2D spectrum without any mixing element and recorded on a 400 MHz spectrometer at 10.0 kHz MAS. The rf field strength of the π-pulses was set to 100 kHz, a XY-8 phase cycling was employed in all experimental approaches. Additional experimental parameters are found in the Experimental section.

Figure 5

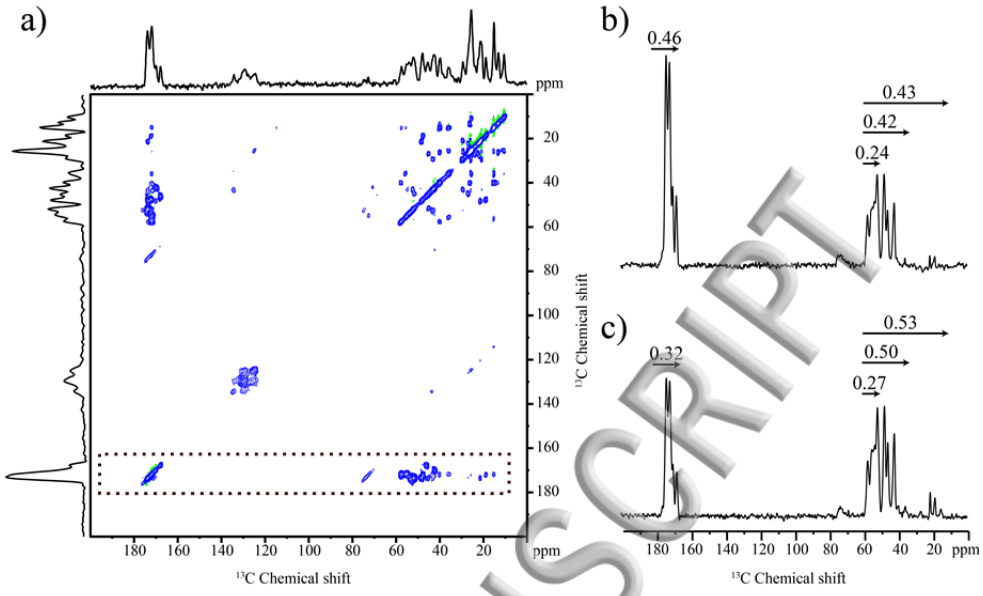

Fig. 5. (a) Experimental 2D ^{13}C-^{13}C correlation spectrum of the peptide SNNFGAILSS uniformly ^{13}C,^{15}N-labeled at the FGAIL residues obtained using the pulse sequence in Fig. 1a with 2.4 ms (24 rotor periods) adiabatic RFDR mixing optimized for most efficient ^{13}CO to ^{13}C$_\alpha$ transfer. The blue and green color represents positive and negative contours, respectively. Sum projections of the carbonyl region in the indirect dimension (see dotted region in (a)) from 2D spectra using (b) 1.2 ms standard RFDR mixing and (c) adiabatic RFDR mixing show the integrated intensities against the diagonal region from a 2D spectrum without any mixing element (Integrated signal from 165.9 to 178.0 ppm from a sum projection in the indirect dimension). The mixing times for both experiments were optimized for the highest ^{13}CO to ^{13}C$_\alpha$ transfer. All data were recorded on a 400 MHz spectrometer at 10.0 kHz MAS. ^{1}H decoupling was employed during the mixing elements using $\omega_{pul}/2\pi$ = 150 kHz and $\omega_{win}/2\pi$ = 90 kHz. A XY-8 phase cycling of the 100 kHz rf amplitude π-pulses was employed for both experiments.

This manuscript was accepted by J. Chem. Phys. Click here to see the version of record.

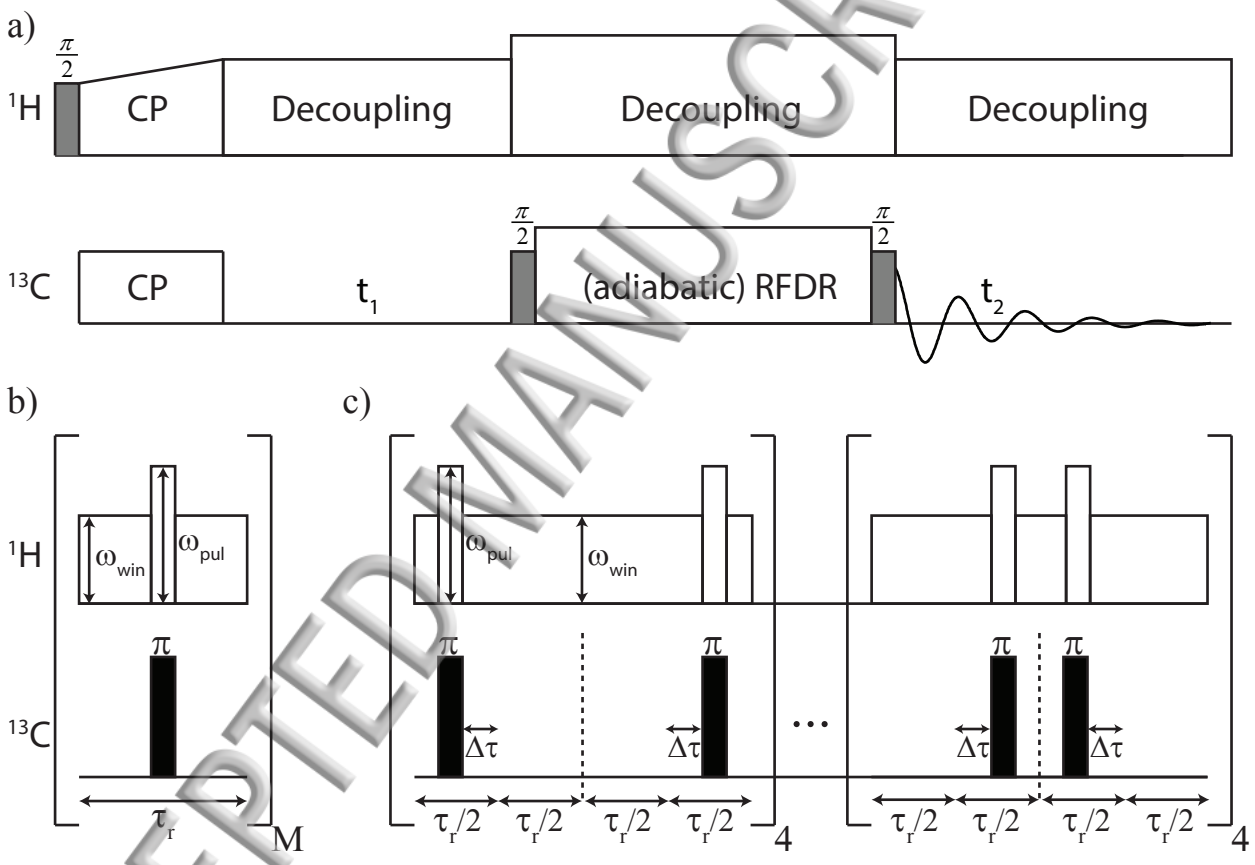

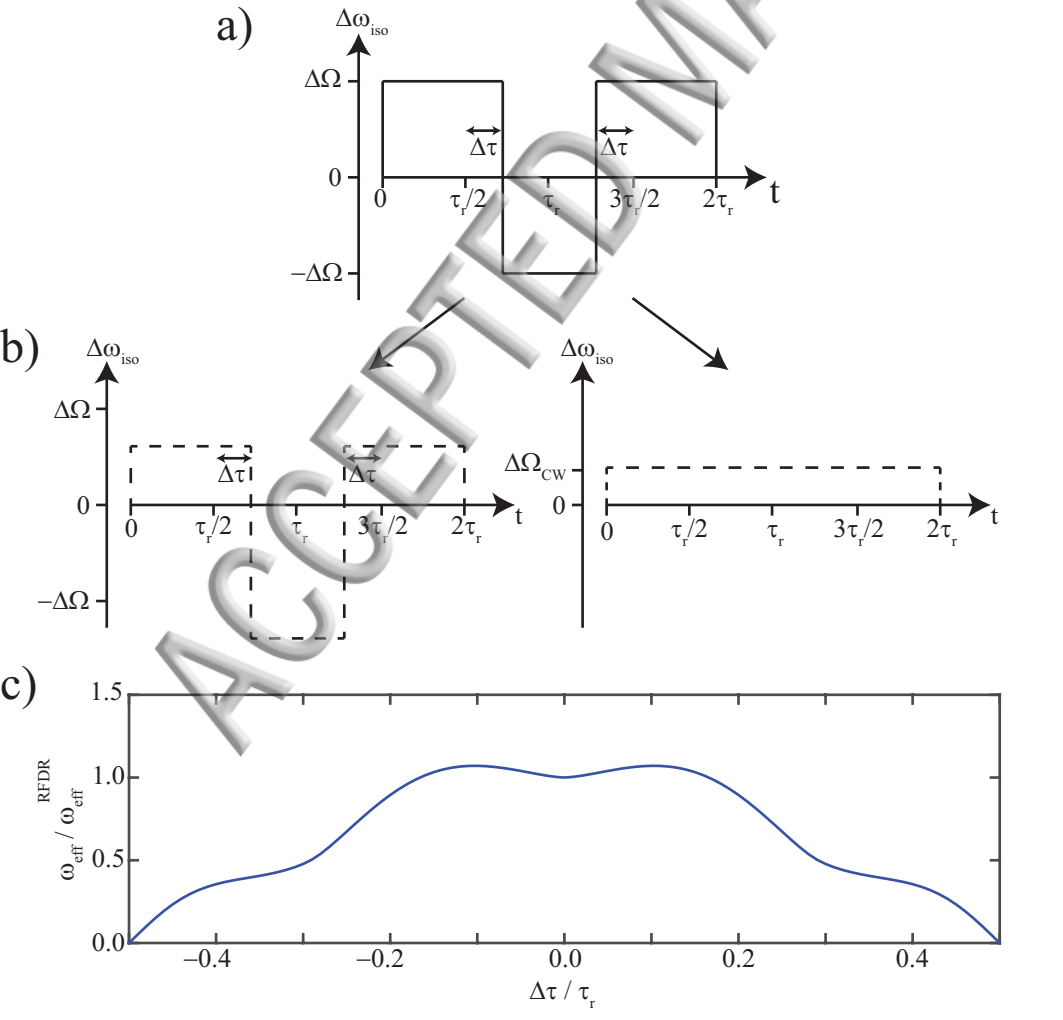
a)
Δω_iso
ΔΩ
0
−ΔΩ
Δτ
Δτ
0
τ_r/2
τ_r
3τ_r/2
2τ_r
t
b)
Δω_iso
ΔΩ
0
−ΔΩ
Δτ
Δτ
0
τ_r/2
τ_r
3τ_r/2
2τ_r
t
Δω_iso
ΔΩ_CW
0
0
τ_r/2
τ_r
3τ_r/2
2τ_r
t
c)
1.5
1.0
0.5
0.0
ω_eff^RFDR / ω_eff
−0.4
−0.2
0.0
0.2
0.4
Δτ / τ_r

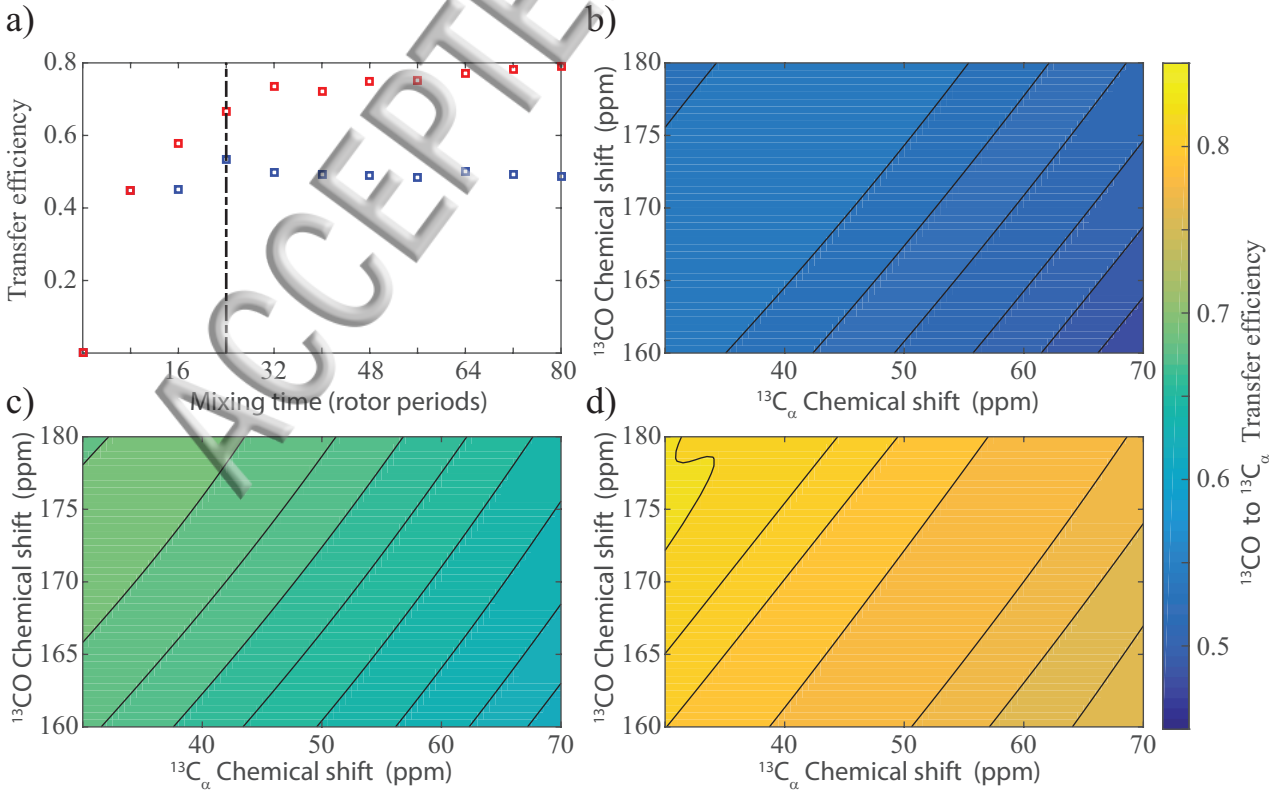
a)
b)
c)
d)
Transfer efficiency
0.8
0.6
0.4
0.2
16
32
48
64
80
Mixing time (rotor periods)
^{13}CO Chemical shift (ppm)
180
175
170
165
160
40
50
60
70
$^{13}C_\alpha$ Chemical shift (ppm)
^{13}CO to $^{13}C_\alpha$ Transfer efficiency
0.8
0.7
0.6
0.5

This manuscript was accepted by J. Chem. Phys. Click here to see the version of record.

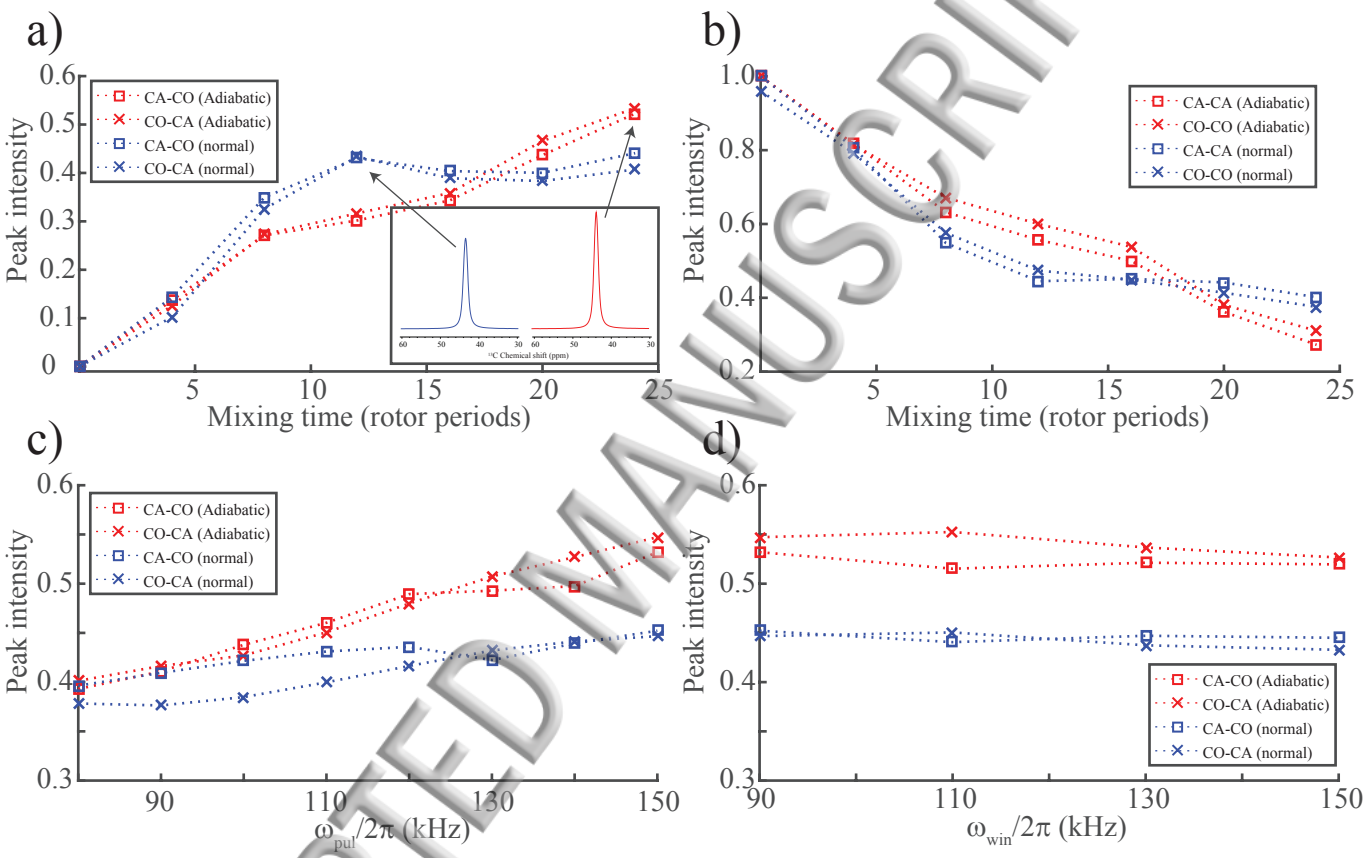

This manuscript was accepted by J. Chem. Phys. Click here to see the version of record.